Construction and Building Materials 411 (2024) 134580

Contents lists available at ScienceDirect

Construction and Building Materials

journal homepage: www.elsevier.com/locate/conbuildmat

Long-term monitoring of a masonry arch bridge to evaluate scour effects

Paolo Borlenghi [a,1], Carmelo Gentile [a,*,2], Manuel D'Angelo [b,c], Francesco Ballio [b,3]

[a] Department of Architecture, Built environment and Construction engineering (DABC), Politecnico di Milano, Piazza Leonardo da Vinci, 32, 20133 Milan, Italy
[b] Department of Civil and Environmental Engineering (DICA), Politecnico di Milano, Piazza Leonardo da Vinci, 32, 20133 Milan, Italy
[c] Tecnoindagini S.r.l., Via Monte Sabotino, 14, 20095 Cusano Milanino, Italy

ARTICLE INFO

Keywords:
Arch bridges
Historical constructions
Inclinometers
Masonry
Novelty detection
Scour
Structural health monitoring
Temperature effects

ABSTRACT

Evaluating the scour effects on masonry arch bridges is of utmost importance to ensure the continued operational safety of those infrastructures. Even if numerical and laboratory studies have demonstrated the possibility of detecting scour-induced effects by measuring the structural response of masonry bridges, there is a lack of long-term monitoring applications on real structures. Within this context, the paper presents selected results obtained during two years of continuous monitoring of a historical masonry arch bridge to evaluate scour-induced effects. Firstly, on-site inspections of the bridge revealed severe foundation erosion and extensive documentary research was carried out to identify the depth of the foundation level. Subsequently, a monitoring system was installed in the bridge, including several MEMS-based tiltmeters, 1 echosounder, 1 hydrometer and 1 weather station. The correlation between measured rotations and environmental parameters is investigated and a linear regression model is used to minimize/remove temperature-induced effects. The residual errors between measured and predicted rotations highlighted the occurrence of various anomalies.

1. Introduction

As highlighted in the scientific literature (see, e.g., [1–3] for the US context and [4,5] for the EU context), about 50–60% of river bridge failures are caused by the soil settlements generated by scour or by other flow-related effects. Notably, the risk of scour-induced collapse is higher in the case of bridges with shallow foundations, such as historical masonry arch bridges. Hence, developing specific monitoring strategies for scour control in masonry bridges is of utmost importance.

Numerical studies have shown that, due to the shallow foundations in the riverbed, a relatively low level of scour may lead to the collapse of masonry arch bridges. Zampieri et al. [6] presented a numerical investigation on a 6-span masonry bridge subjected to incremental scour settlement levels, identifying thresholds that induced the bridge failure. Tubaldi et al. [7] investigated the effects of asymmetric (upstream--downstream) riverbed erosion on a two-span masonry bridge with a novel numerical modelling procedure. The research highlighted that: (a) effects of scouring-induced settlements were related to pier-foundation rotations in the opposite direction of the river flow; (b) the pier displacements started to increase beyond the values induced by vertical loads only after the maximum scour depth exceeds the foundation depth. Invernizzi et al. [8] developed a laboratory-scaled model of a 2-span masonry bridge and applied differential settlements to simulate the effect of scour. Different measurements were performed during the tests, as well as numerical modelling.

Broadly speaking, scour monitoring can be classified into two groups: (1) direct and (2) indirect techniques.

The objective of direct techniques is to measure riverbed variations (in terms of elevation) around pier foundations using underwater sensing devices. Classical direct monitoring techniques include sonars, magnetic sliding collars, float-out devices, and sounding rods. De Falco and Mele [9] used sonar installed on the piers of two railway bridges crossing the Po River (Northern Italy) to measure riverbed variations during floods. Ballio et al. [10] proposed a real-time monitoring strategy for bridge management during extreme events. According to this strategy, the riverbed elevation during flood is measured through an echosounder and a sedimeter (based on fibre optic Bragg gratings), together with a radar water elevation gauge; moreover, 2 cameras and 1 anemometer are used to collect information on debris accumulation and wind characteristics, respectively. Larrarte et al. [11] monitored the

* Corresponding author.
E-mail address: carmelo.gentile@polimi.it (C. Gentile).
[1] ORCID: 0000-0002-6004-5265
[2] 0000-0002-3260-8243
[3] 0000-0002-8499-1707

https://doi.org/10.1016/j.conbuildmat.2023.134580
Received 10 August 2023; Received in revised form 6 November 2023; Accepted 11 December 2023
Available online 19 December 2023
0950-0618/© 2023 The Author(s). Published by Elsevier Ltd. This is an open access article under the CC BY-NC-ND license (http://creativecommons.org/licenses/by-nc-nd/4.0/).

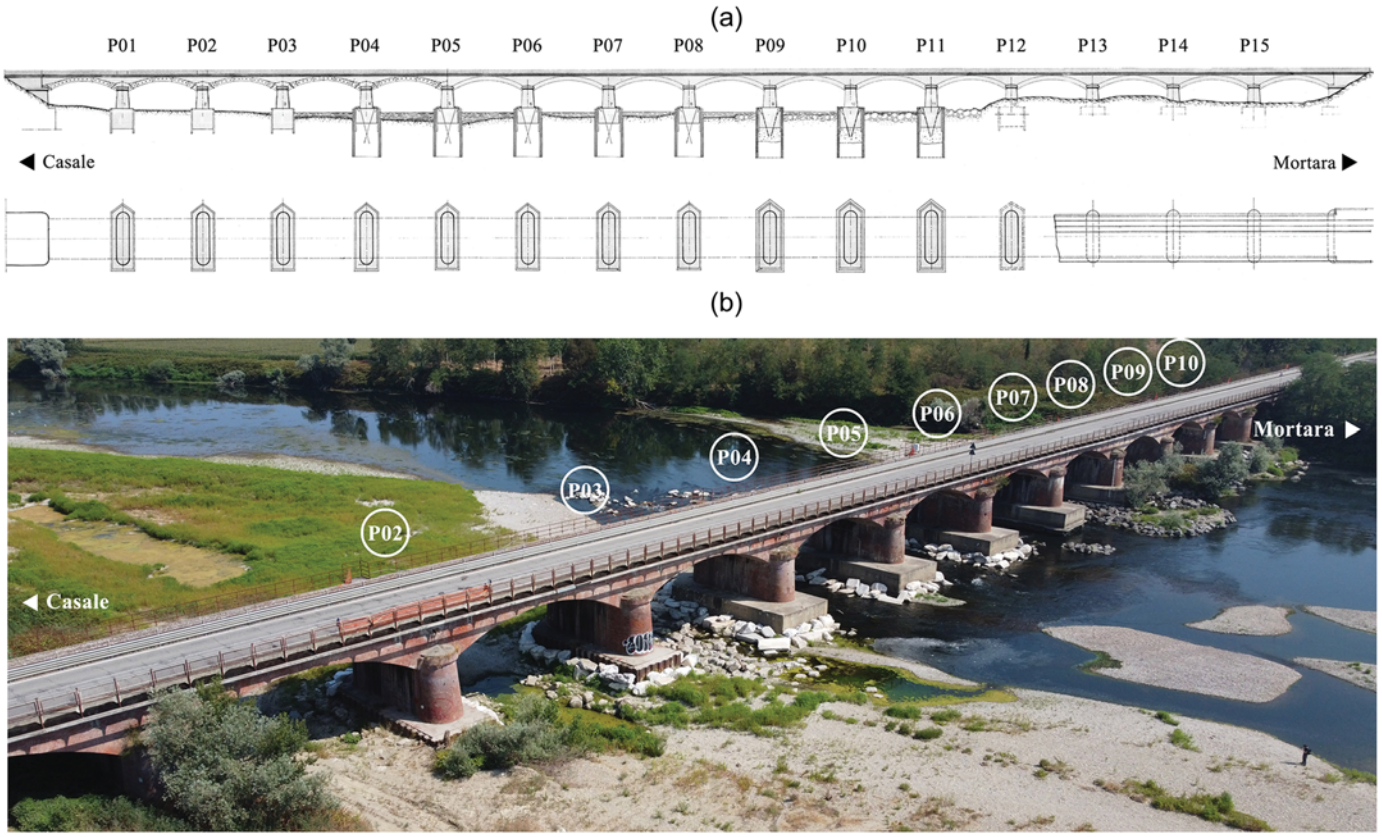

Fig. 1. The Candia Bridge: (a) Plan and elevation from downstream; (b) Aerial view from downstream.

abutment scour of a single-arch bridge using an underwater ultrasonic transducer measuring velocity profile and water depth. Maroni et al. [12] performed two years of riverbed monitoring at the A76 200 bridge over the River Nith, UK – one 3-span stone masonry arch bridge – using two probes buried into the riverbed and equipped with electromagnetic sensors. Other promising applications of local riverbed measurements are illustrated in [13–15].

Indirect monitoring techniques focus on identifying the scour-induced effects on the structural response, mainly using accelerometers (and modal parameters as a scour-sensitive feature) or tiltmeters (and pier rotations as a scour-sensitive feature). Scour usually generates changes in the boundary conditions that might be detected using vibration-based techniques. Foti and Sabia [16] investigated the dynamic response of a multi-span bridge with simply supported girders before and after the retrofitting of a pier affected by local erosion. Scozzese et al. [17] studied a multi-span masonry bridge that partially collapsed due to scour, evaluating the variations of modal parameters for different erosion levels from a calibrated numerical model. Xiong et al. [18] investigated the variations of modal parameters with repeated dynamic testing of the superstructures of a cable-stayed bridge, identifying the scour depth from a calibrated numerical model. Other promising applications of vibration-based methods are illustrated in [19,20]. The use of tiltmeter-based systems for the scour identification is reported in technical reports [21] as well as in research projects [16,22,23]: the most common application is the measure of rotations at the top of the bridges piers.

Overall, the literature review highlighted the presence of numerous studies on the direct measure of scour, while limited long-term monitoring applications have been published on indirect methods. In addition, numerical/laboratory studies on masonry bridges have demonstrated the possibility of detecting scour-induced effects on the structural response. The main aim of the present research is the development and implementation of a monitoring system that merges direct and indirect techniques to highlight the possible effect of scouring on masonry bridges over an extended period. The long-term evaluation of scour action is performed on a historical masonry bridge, called Candia bridge (Fig. 1).

Within a recent research collaboration between Politecnico di Milano and the Lombardy Region about risk-based classification [24] and Structural Health Monitoring of road infrastructures [25], nine bridges were monitored (see, e.g. [26–30]) and the Candia bridge was one of them. The investigated structure is a 19th-century masonry arch bridge crossing the Sesia River in the Province of Pavia (north of Italy). The bridge consists of 16 arches, 15 piers and end abutments. Past inspections revealed that piers foundations resting on the riverbed were subjected to scouring. Subsequently, detailed onsite inspections and extensive documentary research were performed, and a monitoring system based on tiltmeters, an echosounder and different environmental sensors was installed.

The evidence from the first six months of continuous monitoring revealed that the tiltmeters – that were installed at the arch skewbacks on the upstream side to guarantee an adequate protection – measured two different behaviours: the first one associated with global rotations of the foundation-pier-arch system; the second one associated with local rotations of the external arch ring. Subsequently, the recorded global rotations are cleansed from temperature-induced effects, highlighting the occurrence of some permanent shifts.

2. Description of the Candia bridge and preliminary activities

The Candia bridge (Fig. 1) [26] is a multi-span masonry arch bridge that crosses the Sesia River between the municipalities of Candia Lomellina and Casale Monferrato. The structure is 325 m long and is composed of 16 segmental arches, 15 piers and end abutments. All structural components are built in brick masonry. The arches have a span – measured from the arch skewback – of 17.5 m. As shown in Fig. 1,

Fig. 2. Variations of debris accumulation on piers P04 and P05 before and after the flood of October 2020.

Fig. 3. Satellite images of the Sesia River (flow direction from top-left to bottom-right): before (a) and after (b) the rock armour installation around the piers of the left side channel.

all the piers with the footing resting on the riverbed were subjected to the strengthening of the foundation, deepening the (shallow) foundation level of about 8–10 m. The deck width is equal to 10 m and includes a roadway and a railway track, with the latter being inactive since 2010.

2.1. Hydraulic analysis from available documents

The Candia bridge is located 5 km upstream of the Sesia River and Po River confluence. The Sesia River has a meandering channel pattern, which appears planimetrically stable from aerial images observation since 1954. The flow regime of the Sesia River is highly variable, with historical flow discharges ranging between 70 m^3/s and 5000 m^3/s. In case of a 200-year event, corresponding to a discharge of 5000 m^3/s, water can reach an elevation of about 105 m above sea level (asl) and 1 m above the skewback of the bridge arches.

According to Pizarro et al. [31], scour can be classified as (1) natural scour, (2) contraction scour, and (3) local scour. In the case of the Candia bridge, the natural scour is occurring due to a general degradation of the altimetric profile of the Sesia River: along the period 1960–2000, the riverbed lowered for about 2–3 m, resulting in the emergence of the foundation plinths from the riverbed. In addition, scour around the foundation of the piers may occur due to local flow accelerations induced by the obstructions in the riverbed (contraction scour) and for the horseshoe vortices forming at the base of the pier (local scour): the large concrete plinths reduced the free flow cross-section to 13.5 m and are susceptible to local scour. The presence of wood debris can further intensify contraction and local scour processes, and in the case of Candia bridge, the accumulation debris is well-documented: Fig. 2 shows the variations of debris accumulation on piers P04 and P05 between the inspection performed on July 2019 and October 2020. Finally, although the bridge is perpendicular to the general direction of the river, the flow at low stage appears to be skewed (see Fig. 3b). Direction of the flow can change with water stage, and it is presumed to be more perpendicular with the bridge at higher stages. However, erosion may occur more intensively on the lateral edge of the piers.

To summarize, contraction and local scour are expected to occur all around the pier, whenever is not known which of the described phenomena play a major role. Local scour, comprehending local and

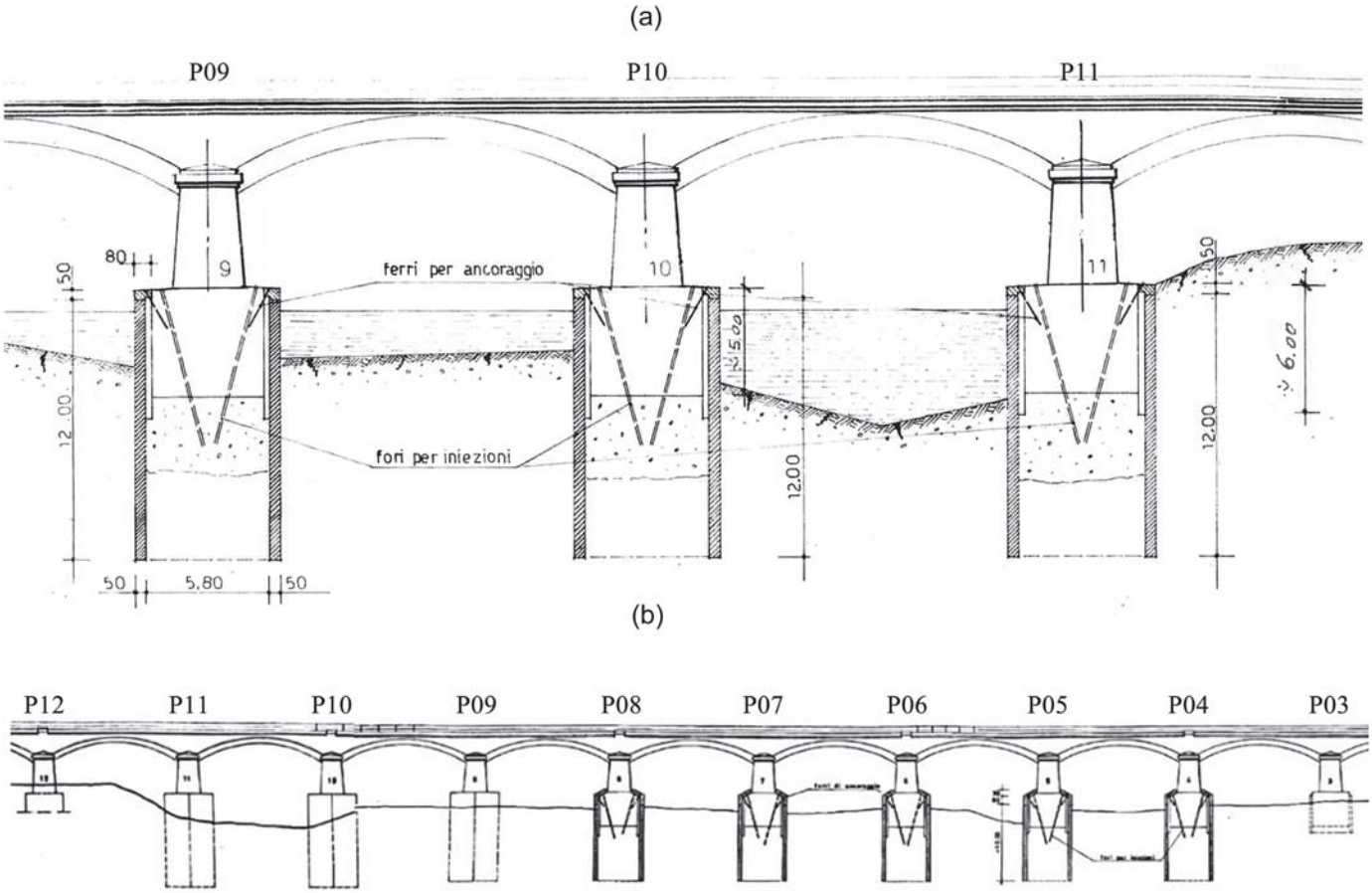

Fig. 4. Historical drawings of different strengthening interventions on the piers: (a) 1955 intervention on piers P09, P10 and P11 (elevation from downstream); (b) 1984 intervention on piers from P04 to P08 (elevation from upstream).

Fig. 5. Foundation scour at pier P08 (picture from the upstream side).

contraction effects, is at some degree expected at any high stage event; general degradation or aggradation of the riverbed, which develop independently of the presence of the bridge, may happen at longer time scales (typically larger than one single high stage event).

Armouring interventions of the riverbed were performed at different times in the attempt to stabilise the sediments around the foundations (Fig. 1). To the authors' knowledge, the last intervention of riverbed stabilisation – before the installation of the monitoring system – was performed in 2003–2004 around the most eroded piers at the left side of the channel, where flow concentrated in normal conditions. This operation, however, modified the local morphology of the riverbed by deviating the main flux from the left-channel (looking downstream) to the central-channel piers, with consequent migration of the thalweg. Fig. 3 compares the satellite images of the Candia bridge of 2002 and 2018, showing a representation of this mechanism.

2.2. Historical research

Due to the lack of available documentation, an extensive documentary research was performed to identify the construction period and the main structural interventions.

The bridge was conceivably built between 1868 and 1870. According to the original design drawings – found in a Thesis of the Royal Technical School of Engineering of Turin [32] – the foundations of the piers were of two types: the piers most exposed to the river flow (at that time), i.e. those on the river right (P01-P04), were founded at a depth of 2 m below the riverbed (96 m asl), while the remaining ones (P05-P15) were founded 1 m below the riverbed (97 m asl). Surprisingly, at the age of the construction, the main river channel was on the river's right. The original shallow foundations were made of concrete and had the following dimensions: (a) width in elevation equal to 4.2 m for P01-P04 and 4.5 m for P05-P15; (b) depth from the top of the plinth equal to 4 m for P01-P04 and 2 m for P05-P15.

Between 1954 and 1955, the 9th arch – included among P08 and P09 – was reconstructed, and the foundations of piers from P09 to P11 were strengthened through a deepening of the foundation level (Fig. 4a) up to 12 m. The reason for the heavy damage to the arch is still unknown, but it was conceivably connected to soil settlements. Subsequently, during the 1980 s, a similar intervention on the foundations of piers P04-P08 was performed (Fig. 4b), together with the strengthening of arches from 1 to 5.

According to the results of the documentary research, the foundation level of piers P04-P11 is equal to approximately 12 m (measured from

(a) Loss of material due to vegetation growth at arch P10-P11

(b) Detachment of the external brick layer at arch P09-P10

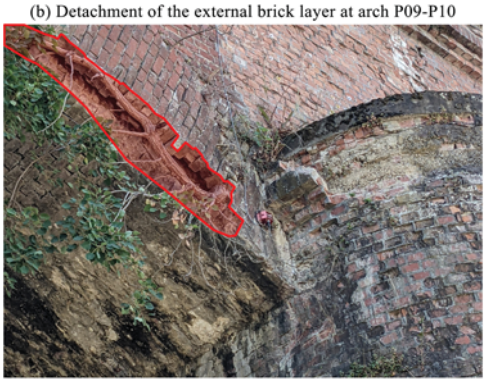

(c) Arch barrel P08-P09: longitudinal discontinuity

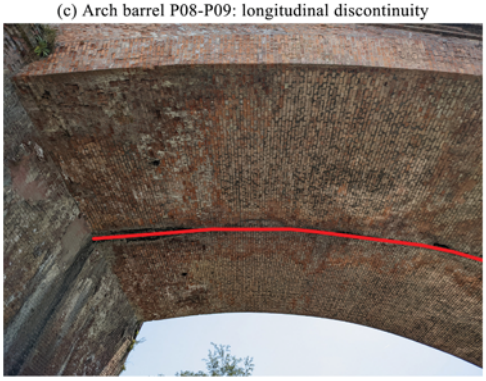

Fig. 6. Damages at the arch barrel of different spans.

the top of the foundation plinth) while the foundation level of piers P01-P03 and P12-P15 is equal to 6 m.

2.3. Onsite visual inspections

The main results of the visual inspections are herein presented. The description of damages and decay phenomena is performed according to the UIC (International Union of Railways) catalogue [33].

As known from past inspections, the most critical defect is the erosion of foundations from pier P09 to pier P04 (Fig. 5) caused by the sum of natural scour – estimated at approximately 3 m drop of riverbed level compared to the year of construction – added to contraction and local scour caused by flow obstruction due to the presence of the piers themselves.

The arch barrels are generally characterised by superficial damages that affect the durability such as black crust, differential surface weathering, efflorescence, and stains near the drainage pipes or near missing portions of masonry.

The vegetation growth has caused the loss of masonry material from the arch barrel. The phenomenon is particularly intense in the arches included between pier P10 and pier P12, where the masonry detachment reduced the thickness of the arch barrel near the skewback line (Fig. 6a).

The arch barrel between piers P08 and P09 shows a longitudinal discontinuity on the entire arch length with a thickness of the order of 1–2 cm (Fig. 6c). This arch was presumably rebuilt in the 1954 intervention, and it is probable that – due to constructive reasons – it was built in two stages using the same centring. The hypothesis of the reconstruction is confirmed by the different consistency of the bricks, lighter and more prone to surface weathering than the original ones.

Another damage affecting durability is the presence of longitudinal cracks in the intrados of the arch barrel below the external covering arch. In brick masonry arch bridges, the covering arch is a coating of one or more layers of bricks covering the arch barrel on the outer vertical faces. As reported in historical manuals (see, e.g., Curioni [34]), it was common to use this technique to obtain a better aesthetic result. In the case of Candia Bridge, the presence of the covering arch is revealed by the decay of arch P09-P10, in which the vegetation growth caused the complete detachment of the first layer of bricks (Fig. 6b).

At last, vertical cracks were detected at the centre of some piers. However, it should be noted that no cracks were identified on the arch barrels except for the structural discontinuity of arch P08-P09 and the longitudinal cracks due to the detachment of external brick layers.

In October 2020, a severe flood of the Sesia River occurred (Fig. 7). The maximum water level reached during the flood can be estimated from available photos, and it is almost equal to 105 m asl (i.e., the elevation of the 200-year flood event). The flood caused severe damage to streets, railway tracks and buildings in the areas nearby the bridge. After the event, the bridge remained closed for over a month.

(a) View during the 2020 flood of the Sesia River

(b) Collapse of the road embankment after the flood

Fig. 7. Effects of the 2020 flood.

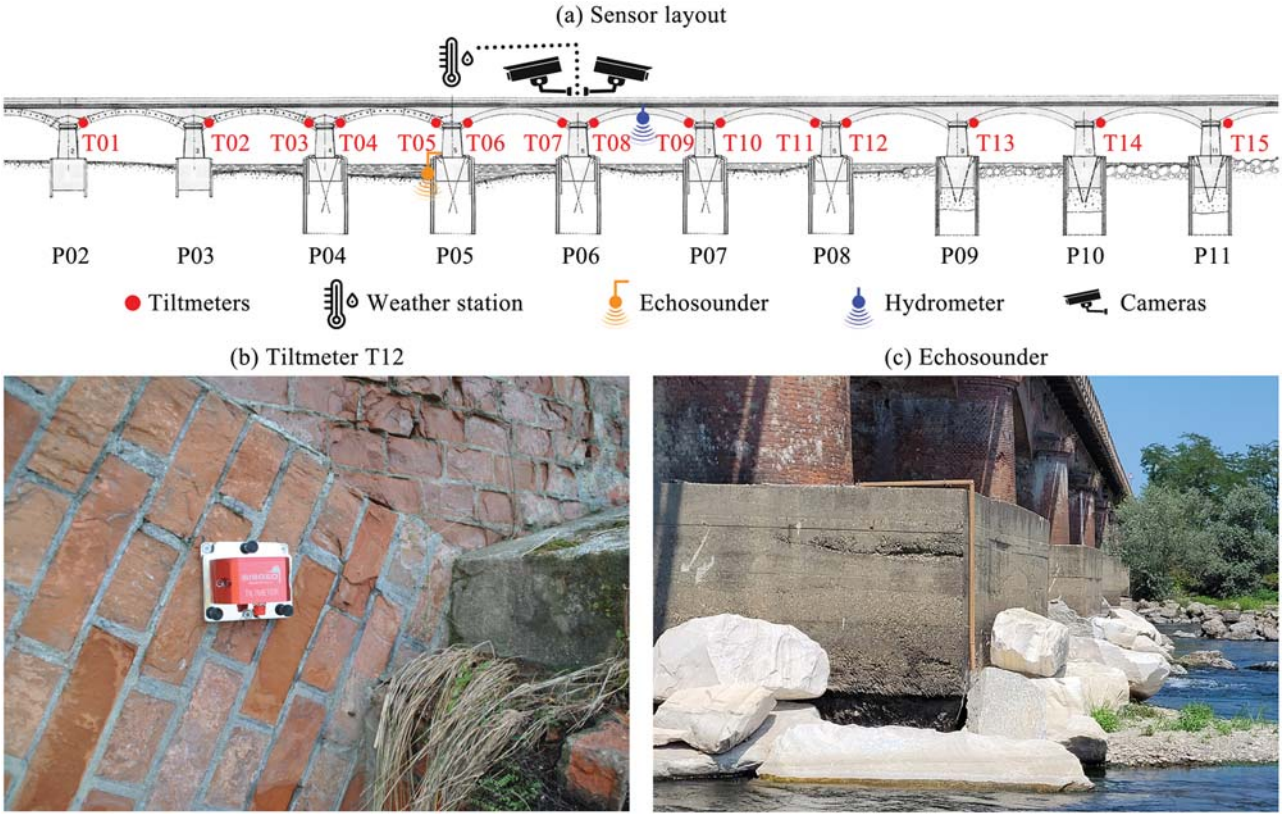

Fig. 8. The monitoring system of the Candia bridge: (a) sensors layout (elevation from downstream); (b) mounting of tiltmeter T12; (c) position of the echosounder on pier P05.

Visual inspections were performed to check whether the high-stage flow induced some damage to the bridge, together with field measurements of riverbed elevation around the piers with a stadia rod. No evidence of significant damage was detected on the bridge. Regarding the riverbed level, the local measures on pier P05 – taken from the top of the foundation plinth – resulted in 5.5 m at the upstream and 2.7 m at the downstream sides: hence, a more intense removal of riverbed sediments is detected on the upstream side [7]. Note also that the scour depth during the highest peak of the event was probably deeper since, generally, the scour holes are partially refilled when the river returns to its ordinary regime.

3. Monitoring system and data analysis

The monitoring system of the Candia bridge is aimed at detecting and localising the structural damages induced by scour. The monitoring system design accounted for both the expected collapse mechanism and the constraints due to possible debris accumulation on the upstream side.

As previously pointed out, the onsite measurements of water depth on pier P05 highlight that the scour is more intense on the upstream side, generating a possible differential settlement of the pier footings. Consequently, the expected collapse mechanism might be induced by the transverse rotation of the foundation-pier-arch system in the opposite direction of the river flow [7]. The monitoring system was indeed designed to measure the transverse rotation of the foundation-pier-arch system using high-sensitivity tiltmeters together with the measure of main environmental parameters for correlation analysis (i.e., outdoor temperature, humidity, water level and riverbed variations).

The monitoring system (Fig. 8) includes: (a) 15 uniaxial MEMS tiltmeters (SISGEO model 0S541MA0202, accuracy $\pm 0.008°$) with integrated temperature sensor; (b) 1 weather station measuring temperature, humidity, rainfall intensity, wind speed and wind direction; (c) 1 hydrometer; (d) 1 echosounder and (e) 2 cameras. The sensors are wired to a data acquisition unit equipped with a modem for data transmission.

Although the ideal position for the tiltmeter installation was the base of the piers, that position cannot allow adequate protection of the sensors from debris accumulation (Fig. 2); hence, it was decided to install the tiltmeters at the arch skewbacks (Fig. 8b). As shown in Fig. 8a, the tiltmeters were installed only on the piers P02-P11 located in the riverbed- Furthermore, the piers from P04 to P08 (i.e., the piers being most affected by the deviation of the river flow from the left- to the central-channel, Fig. 3) are monitored with two tiltmeters, one for each skewback.

In addition to the weather station, the outdoor temperatures are also measured by the internal thermistor of the tiltmeters. The water level is measured by a hydrometer positioned at the deck level, whereas the evolution of scouring holes is tracked with an echosounder.

The echosounder has been installed to capture the effects of the sediment transport processes described in subsection 2.1. Single point measurements are able to identify aggradation and erosion processes at a peculiar position of the pier, whilst it cannot distinguish among contributions of the individual processes occurring at the bridge. As shown in Fig. 8c, the echosounder is installed on the foundation plinth of pier P05 on the downstream side, at the right corner (with respect to the water flow): of course, the ideal position should be on the upstream side (where the maximum scour depth may occur) but the possible debris accumulation on that side suggested the installation on the opposite downstream side. In this position, the flow hydrodynamics is affected by the wake of the pier itself. Hence, the positioning on the corner was thought to be able to detect an area where flow velocity is not close to zero. However, aggradation may occur at the downstream edge of the pier for the wake effect of the pier. Nonetheless, the measurements

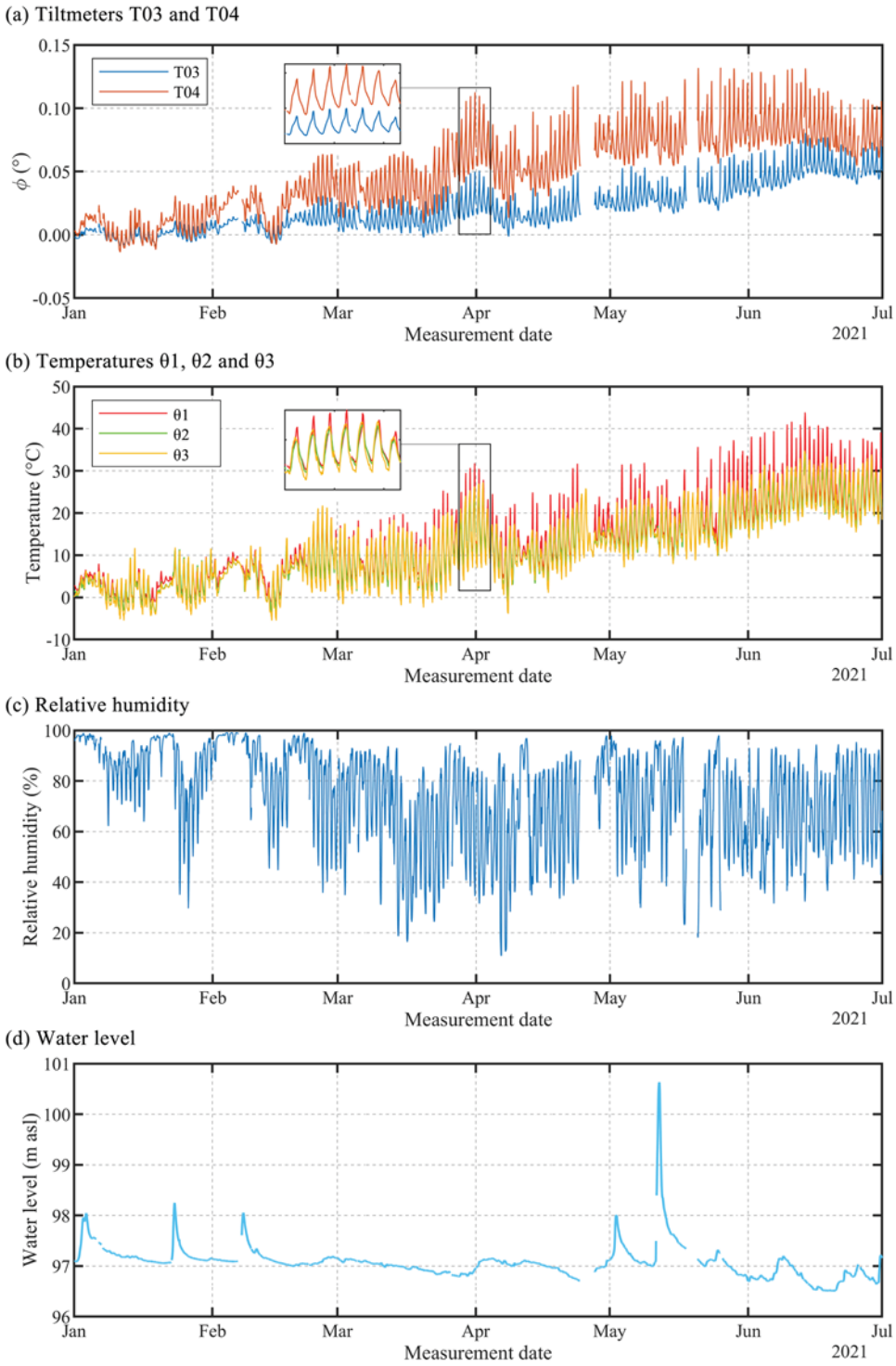

Fig. 9. Time period from 01/01/2021 to 30/06/2021. Evolution in time of: (a) rotations at pier P04 (tiltmeters T03 and T04); (b) outdoor temperature at different locations; (c) relative humidity and (d) water level.

provide valuable information, being able to clarify for which water levels sediment transport occurs. It is worth mentioning that the echosounder only measures the riverbed level when underwater. In the present case, the echosounder at pier P05 goes underwater only when the water level exceeds 97.5 m asl, half a meter above the ordinary regime of the river.

It is further noticed that the debris accumulation at the piers is detected with 2 cameras taking pictures along the upstream side of the bridge.

The continuous monitoring system has been active since November 22nd, 2020. The sensor network works at a sampling frequency of 1 Hz, with the exception of the cameras, that take pictures every 10 min. The recorded data are collected every hour in 1 binary file that is sent to Politecnico di Milano for analysis. The processing of structural (rotations) and environmental data includes the following steps: (a) check the completeness of the hourly files (the monitoring system is restarted every week to avoid memory issues); (b) average the data to obtain a single observation per hour. A different approach is adopted for the

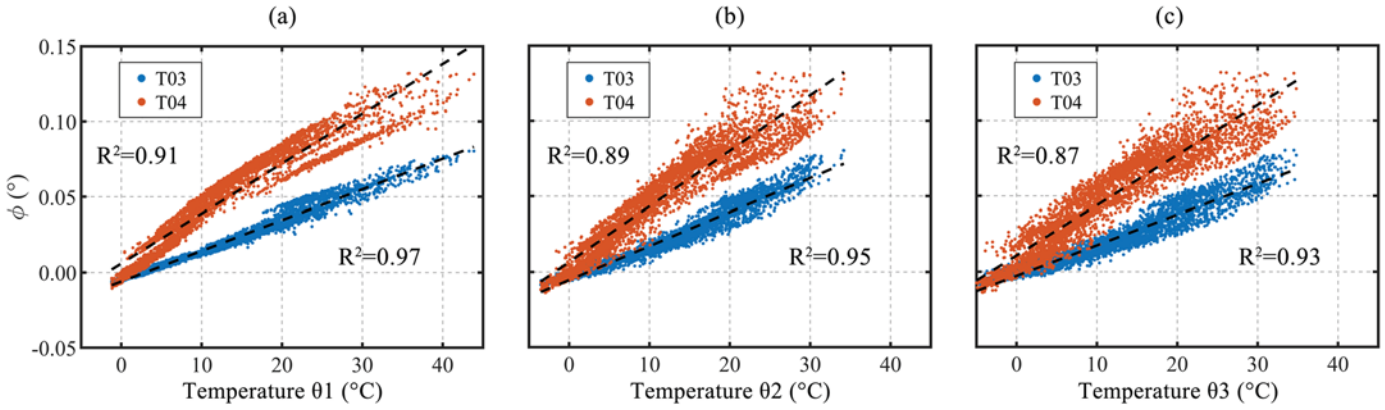

Fig. 10. Correlations between the rotations T03 and T04 and different outdoor temperatures: (a) surface temperature at upstream (θ1); (b) bridge weather station (θ2); (c) local weather station (θ3).

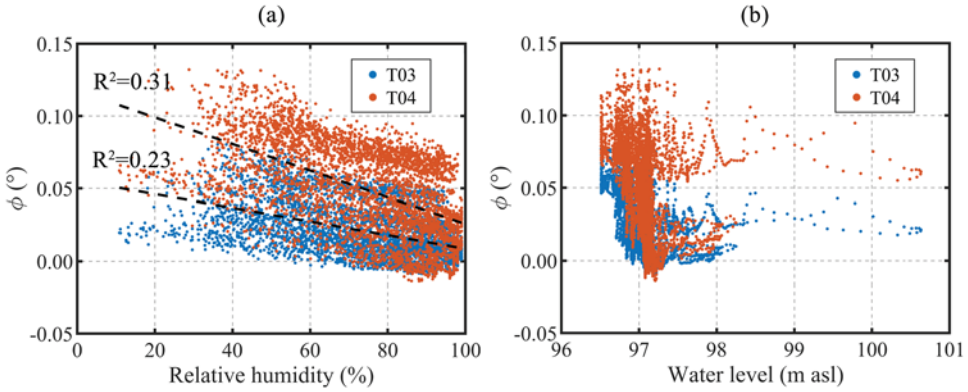

Fig. 11. Correlations between the rotations T03 and T04 and (a) relative humidity and (b) water level.

echosounder data: as known from the literature [35], the echoes due to air bubbles, suspended sediments and turbulences generate fake echoes that need to be removed. To this purpose, the riverbed level is reconstructed, removing the "fake echoes": the outliers are defined as measurements with more than three local standard deviations from the local mean over a window length of 3600 s [36].

The measured rotations are affected by temperature-induced variations and those variations should be identified and removed to detect the onset of abnormal variations. To this purpose, a simple linear regression is adopted and calibrated during a training period of 6 months. As long as the structure exhibits regular behaviour without any anomalies, the regression model can predict the evolution of structural rotations. Once the rotations deviate from the regular behaviour, the residuals between predicted and measured rotations are used to detect the anomaly.

4. Evidences provided by the first six months of monitoring

Selected results obtained in the first period of continuous monitoring – namely from January 1st, 2021 to June 30th, 2021 – are herein presented to highlight some peculiarities of the monitored parameters. It is worth mentioning that during the monitoring period, a few malfunctions in the data acquisition system – solved by an automatic reboot every week – generated the missing values in Fig. 9.

The evolution of structural rotations is exemplified in Fig. 9a by the measurements of tiltmeters T03 and T04. It should be noticed that positive rotations correspond to transverse rotations of the arch-pier system towards the downstream. The inspection of Fig. 9a allows to observe that rotations tend to increase with increased temperature, with this observation being confirmed by the comparison with the temperature evolution (Fig. 9b). Figs. 9a and 9b also show the daily fluctuation of rotations and temperatures by zooming one week of data (between March 28th and April 4th) and again positive correlation is observed between rotations and temperatures.

Fig. 9b shows the evolution of the outdoor temperature in three different locations: (a) θ1 refers to the external surface of the bridge at tiltmeter T14; (b) θ2 is related to the weather station (i.e., extrados of the bridge deck) and (c) θ3 refers to the closest ARPA (i.e., the Agency for Environmental Protection of the Lombardy Region) weather station, about 13 km far from the bridge. The measured temperature fluctuations are $-1.2\,^{\circ}C \leq \theta1 \leq 43.9\,^{\circ}C$, $-3.5\,^{\circ}C \leq \theta2 \leq 34.2\,^{\circ}C$ and $-5.5\,^{\circ}C \leq \theta3 \leq 34.8\,^{\circ}C$: hence, the selected time period includes a statistically representative sample of the expected environmental conditions.

Figs. 9c and 9d show the evolution of the relative humidity (weather station) and water level (hydrometer), respectively. Fig. 9d indicates that, in the investigated time period, the average water level was about 97.0 m asl (i.e., 8 m lower than the elevation of the 200-year flood event), with the maximum measured level of 100.6 m asl being reached on May 12th, 2021. According to a hydrological analysis carried out after the event, the associated return period for the 100.6 m water level was less than 2 years. Hence, no relevant events were recorded during this time period.

Regarding the riverbed elevation, due to the malfunctioning of the echosounder, the first measurements were performed at the beginning of June 2021. Consequently, the echosounder measurements are not addressed in the present section.

Fig. 10 shows the correlation between the rotations measured by tiltmeters T03 and T04 and the outdoor temperatures θ1, θ2 and θ3, highlighting that temperature is a dominant driver of rotation variability. In addition, the coefficient of determination R^2 show the best fit

Table 1
Statistics of the measured rotations from 01/01/2021 to 30/06/2021 and correlation analysis with different environmental parameters.

	Tiltmeter Id.	φ_{ave} (°)	$\varphi_{\lvert max \rvert}$ (°)	σ_{φ} (°)	$R^2_{(Ti,\theta1)}$ (−)	$R^2_{(Ti,\theta2)}$ (−)	$R^2_{(Ti,\theta3)}$ (−)	$R^2_{(Ti,RH)}$ (−)	$R^2_{(Ti,WL)}$ (−)
Global rotations	T02	0.017	0.090	0.022	0.920	0.872	0.862	0.262	0.065
	T03	0.021	0.080	0.019	0.974	0.953	0.928	0.231	0.108
	T04	0.049	0.132	0.031	0.911	0.893	0.874	0.309	0.056
	T07	0.020	0.084	0.017	0.915	0.856	0.842	0.287	0.079
	T08	0.021	0.070	0.018	0.918	0.892	0.872	0.207	0.080
	T12	0.011	0.099	0.022	0.938	0.880	0.883	0.312	0.094
Local rotations	T01	-0.005	0.033	0.007	0.832	0.780	0.796	0.277	0.035
	T05	0.009	0.018	0.007	0.249	0.244	0.241	0.013	0.130
	T06	-0.001	0.030	0.008	0.795	0.759	0.739	0.136	0.149
	T09	0.016	0.045	0.008	0.032	0.028	0.034	0.197	0.015
	T10	-0.009	0.040	0.008	0.676	0.653	0.620	0.377	0.045
	T11	-0.009	0.035	0.006	0.000	0.004	0.002	0.001	0.014
	T13	0.002	0.013	0.004	0.653	0.642	0.622	0.089	0.030
	T14	-0.011	0.022	0.005	0.725	0.763	0.745	0.215	0.053
	T15	-0.010	0.023	0.008	0.436	0.393	0.392	0.020	0.059
	Mean	0.014	0.054	0.013	0.665	0.641	0.630	0.196	0.068

θ1 = temperature measured at tiltmeter T14
θ2 = temperature measured by the bridge weather station
θ3 = temperature measured by the ARPA weather station
RH = relative humidity
WL = water level

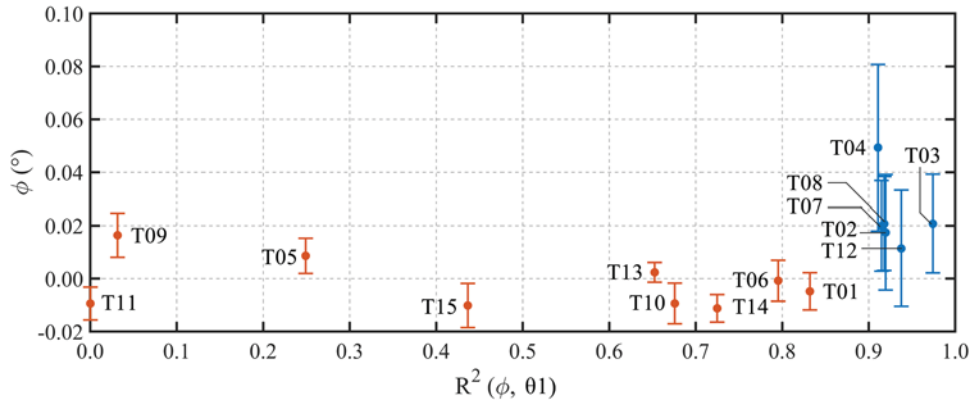

Fig. 12. Identification of global and local rotations in the time period January-June 2021 (error bars indicate the standard deviation).

for θ1, namely the temperature measured on the bridge surface. Consequently, only θ1 is considered for correlation analysis in the subsequent sections.

Fig. 11 shows the correlation between T03-T04 and relative humidity (Fig. 11a) and water level (Fig. 11b), respectively. The inspection of Fig. 11 reveals: (a) the absence of a correlation between rotations and water level (Fig. 11b), despite the relatively important hydraulic event of May 2021 (+3.6 m over the average water level) and (b) the relatively poor rotation-humidity correlation (Fig. 11a), indicated by R^2 coefficient equal to 0.23 for T03 and 0.31 for T04. In addition, the rotation-humidity correlation is conceivably driven by the temperature-humidity relationship, which is characterized by the R^2 value of 0.29.

Based on the previous results, the removal/minimization of environmental effects, addressed in Section 5, is based only on θ1.

Table 1 shows the statistics of the measured rotations for the selected period in terms of average values (φ_{ave}), absolute maximum values ($\varphi_{|max|}$), standard deviations (σ_{φ}) and coefficient of determination R^2 computed with respect to different measured environmental parameters.

From the statistical analysis, it is possible to identify two main behaviours in the rotation data:

(1) rotation-temperature (θ1) correlation with $R^2 > 0.9$ and standard deviation $\sigma_{\varphi} > 0.01°$;

(2) rotation-temperature (θ1) correlation with $R^2 < 0.9$ and standard deviation $\sigma_{\varphi} < 0.01°$.

Lower correlation and lower amplitude variations, as well as lower average values, can be associated with a local rotation of the external arch ring, while the other data can be associated with rotations of the entire foundation-pier-arch system. The variations of outdoor temperatures generate deformations and rotations in the structure. Those deformations are expected to be higher in case more material is involved in the process. Supposing that the external arch ring is entirely detached from the structure (see, e.g. T13), it can be expected that the mean rotation values (as well as the standard deviations) are lower than the rotations of the entire foundation-pier system (see, e.g. T04). In addition, if the external arch ring is detached from the vault or damaged, a non-linear behaviour can be expected and, consequently, a poor correlation with temperature.

Consequently, behaviour (1) is associated with global rotations, while behaviour (2) is associated with local rotations. The identification of global/local rotations is even more evident in Fig. 12: measured global rotations are well correlated with temperature and have larger oscillation (σ_{φ}) and larger values (φ_{ave}), while local rotations exhibit the opposite behaviour.

The tiltmeters measuring local rotations are not addressed in the following since the objective is investigating the possible effects of scour-induced settlements.

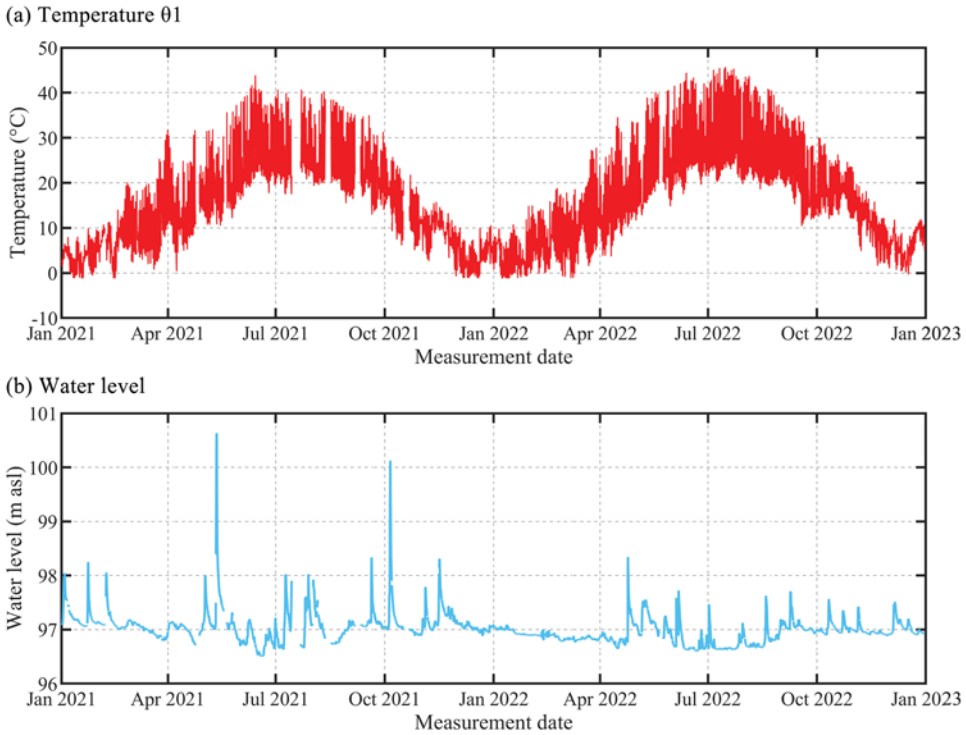

Fig. 13. Variation in time of temperature θ1 (a) and water level (b) from 01/01/2021 to 31/12/2022.

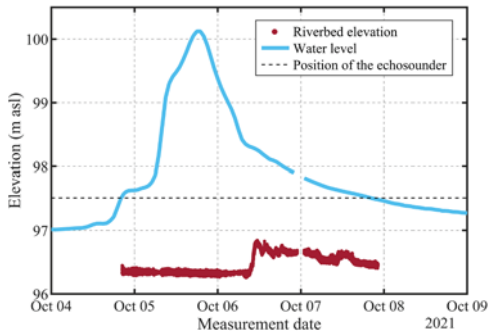

Fig. 14. Variation in time of the riverbed elevation during the hydraulic event of October 2021.

5. Long-term monitoring results and discussion

In the present section the main results of the long-term monitoring are presented for a period of 2 years, from 01/01/2021 to 31/12/2022. In more details, the discussion focuses on the measured global rotations as defined in Section 4. During the investigated 2 years of monitoring, 17520 1-h datasets were collected and processed together with the upstream side pictures taken with the permanent cameras in the daylight.

5.1. Environmental parameters

The variation in time of temperature θ1, turning out to be the main driver of the rotation changes, is shown in Fig. 13a and ranges between − 1.2 °C and 45.7 °C. Fig. 13b presents the time evolution of the water level and shows an average level that is practically equal to the one of the training period (97.0 m, see Fig. 9d). It is further noticed that, during the first two years of monitoring, two high stage hydraulic events were observed, in May and October 2021: the corresponding water level (Fig. 13b) reached 100.6 m asl and 100.1 m asl, respectively. However, as previously stated, these events had a return period smaller than 2 years. Hence, during the two years of monitoring, the bridge has not encountered severe events like the one in 2020 mentioned in subsection 2.3.

During the second event, the echosounder was active and Fig. 14 shows the evolution of the riverbed elevation measured by the echosounder installed in the foundation of pier P05 on the downstream side. It should be noticed (Fig. 14) that the riverbed elevation of 96.3 m asl did not increase during most of the event, whereas an aggradation process was observed during the descending phase, with an increase of 50 cm of the riverbed elevation. Hence, the measured data suggests that the downstream side of the bridge foundations is mainly subjected to the deposition of sediments during major hydraulic events rather than excavation. Of course, this conclusion should be confirmed by further measurements.

Fig. 15. Debris accumulation process at pier P05 on May 12th, 2021.

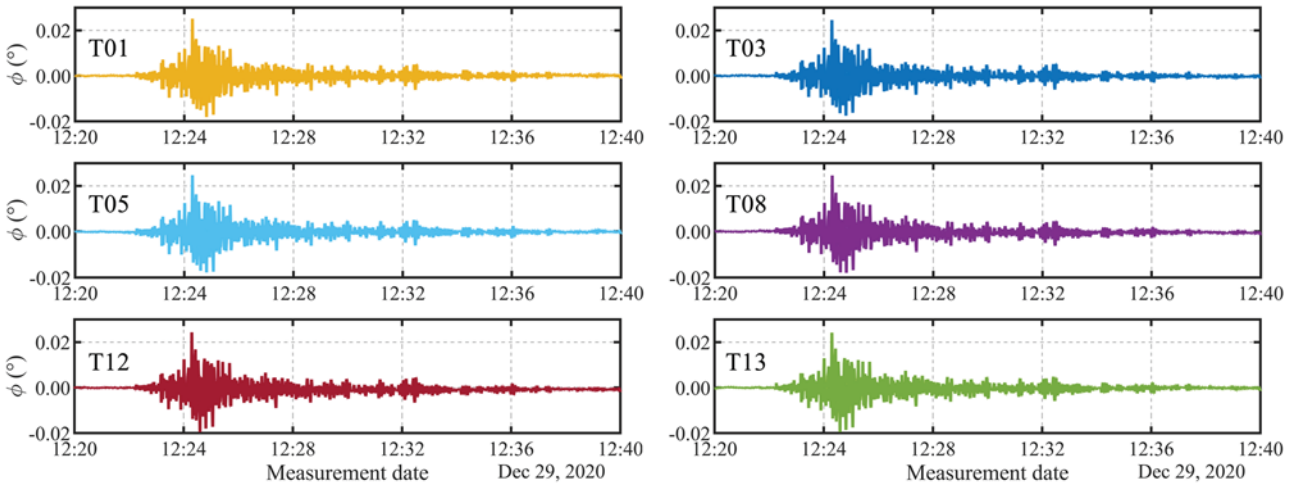

Fig. 16. Selected rotation time series collected during the seismic event of December 29th, 2021 (Petrinja earthquake, Croatia, Mw=6.3).

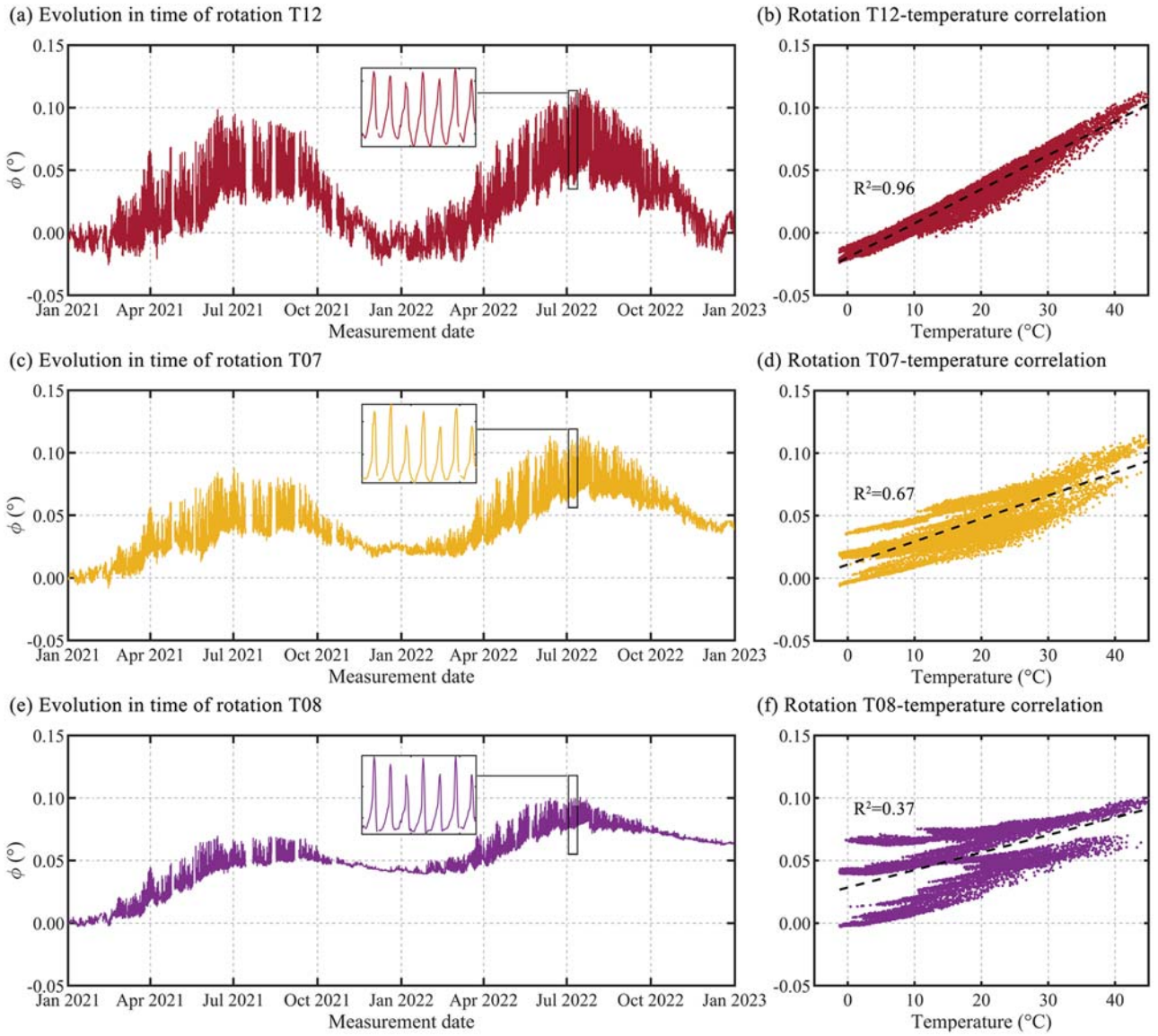

Fig. 17. Variation in time of rotation and rotation-temperature correlation of selected tiltmeters: (a-b) T12, (c-d) T07, (e-f) T08.

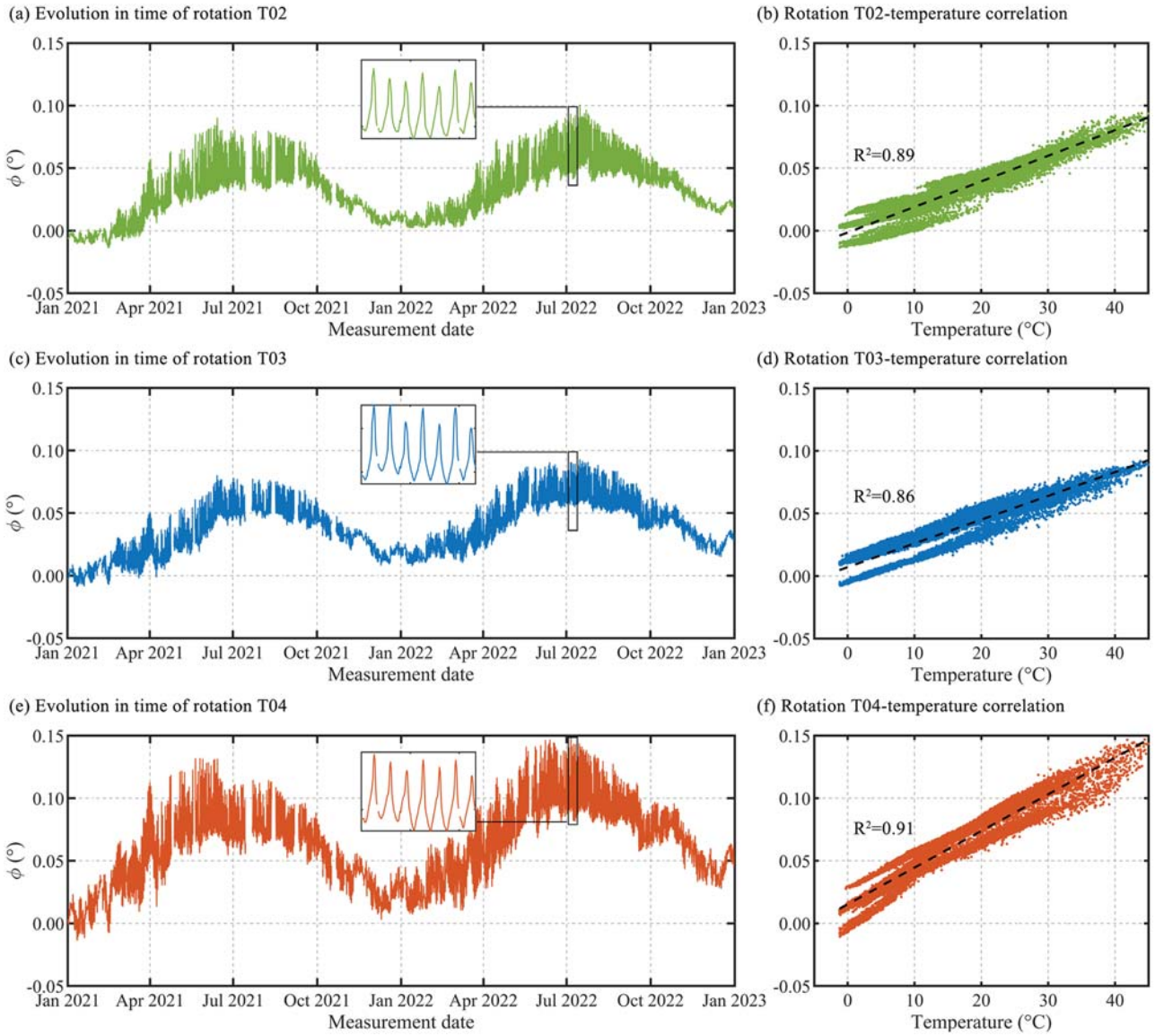

Fig. 18. Variation in time of rotation and rotation-temperature correlation of selected tiltmeters: (a-b) T02, (c-d) T03, (e-f) T04.

Table 2
Statistics of the measured rotations from 01/01/2021 to 31/12/2022.

Tiltmeter Id.	φ_{ave} (°)	$\varphi_{\|max\|}$ (°)	σ_{φ} (°)	$R^2_{(Ti,01)}$ (−)
T12	0.022	0.116	0.027	0.961
T07	0.039	0.114	0.022	0.669
T08	0.050	0.101	0.023	0.366
T02	0.030	0.101	0.021	0.893
T03	0.036	0.093	0.020	0.864
T04	0.060	0.148	0.030	0.913

It is worth mentioning that in January 2022, a new rip-rap protection was installed around the foundations of pier P04-P07 (white stones in Fig. 1b); after the intervention, no appreciable changes in the riverbed elevation were measured. On the other hand and as anticipated in Section 4, the measured rotations were not affected by water level or riverbed elevation during the examined monitoring period.

5.2. Debris accumulation

When arch bridges are characterized by relatively short spans, the risk of occlusion of some spans becomes not negligible. In addition, debris accumulation increases the effect of scour around piers because the occlusion of one or more spans results in an increase of flow velocity under the remaining free spans. Hence, two cameras were installed on pier P06 and pier P07, filming the right and left upstream sides of the river, respectively. To understand the mechanism of debris accumulation, the cameras collected pictures every 10 min.

Accumulation of debris was observed in several events, typically when water reached the upper edge of the foundation plinth. Fig. 15 shows the accumulation process at pier P05 occurred in May 2021. It can be observed the debris mat increases in size, reaching its final configuration during the peak of the event.

The long-term visual monitoring confirmed the importance of the debris accumulation process in the case of Candia bridge and the process was observed also during events having relatively low return period, such as the one recorded in May 2021.

5.3. Monitored (global) rotations

5.3.1. Recorded seismic events

Various far-field earthquakes occurred during the monitoring period. As an example, Fig. 16 shows selected recorded time series of structural

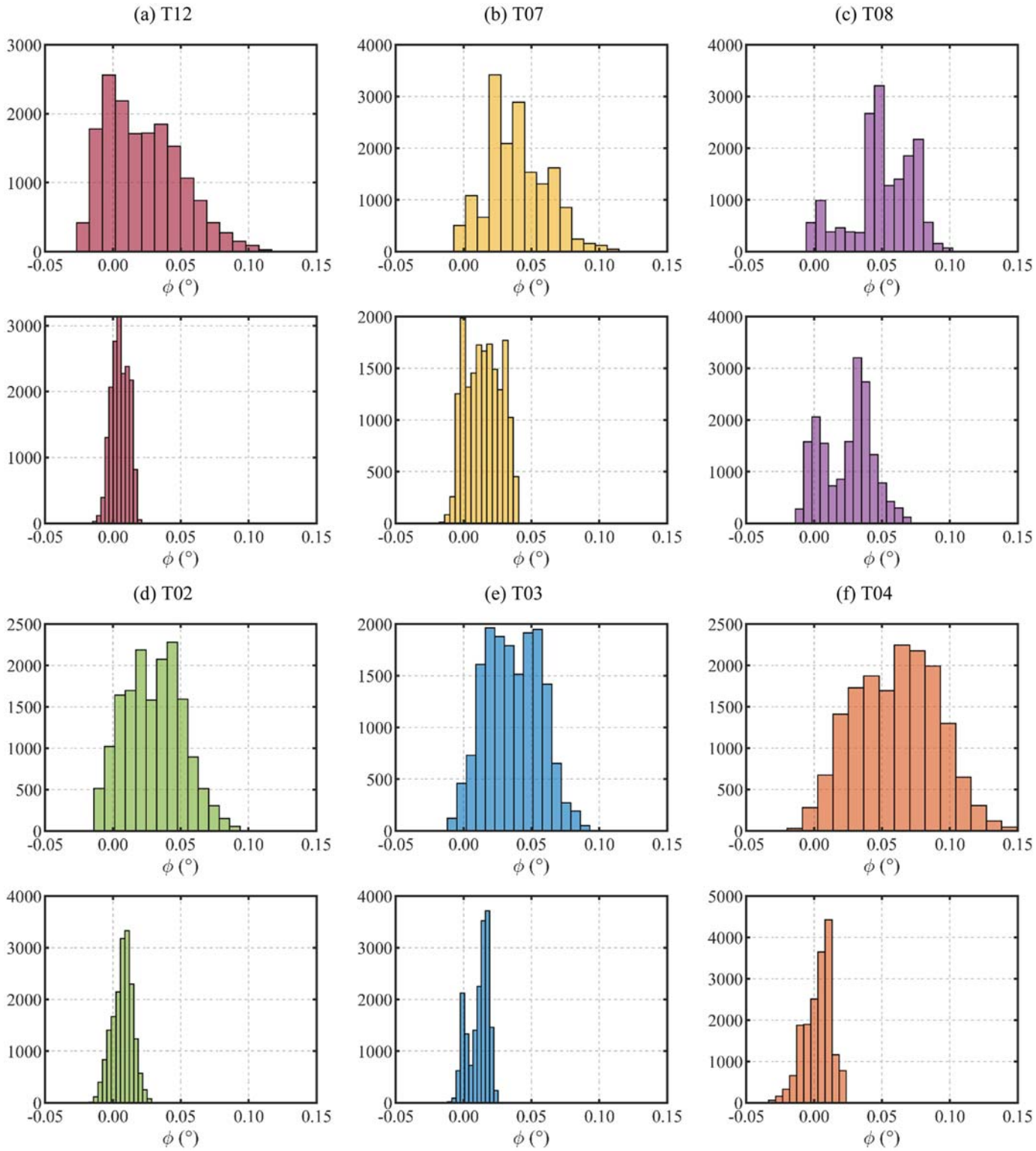

Fig. 19. Histograms of the global rotations before and after the removal of environmental effects.

rotations during the Petrinja earthquake in Croatia (Mw=6.3) on December 29th, 2021. Since the sampling frequency is 1 Hz, the recorded signals are affected by aliasing; however, it is interesting to note that all tiltmeters recorded similar responses, with no permanent rotation being observed after the seismic sequence.

5.3.2. Global rotations

As previously pointed out (Fig. 12), tiltmeters T02, T03, T04, T07, T08 and T12 measure global rotation of the arch-pier system. The variation in time of the rotations of those tiltmeters, as well as the rotation-temperature correlation, is summarized in Figs. 17 and 18. As observed in the first months of monitoring, the structural rotations of the arch-pier system tend to increase during the summer while decreasing during the winter, with an approximately linear dependence on temperature θ1. The inspection of Fig. 17 and Fig. 18 allows the following comments.

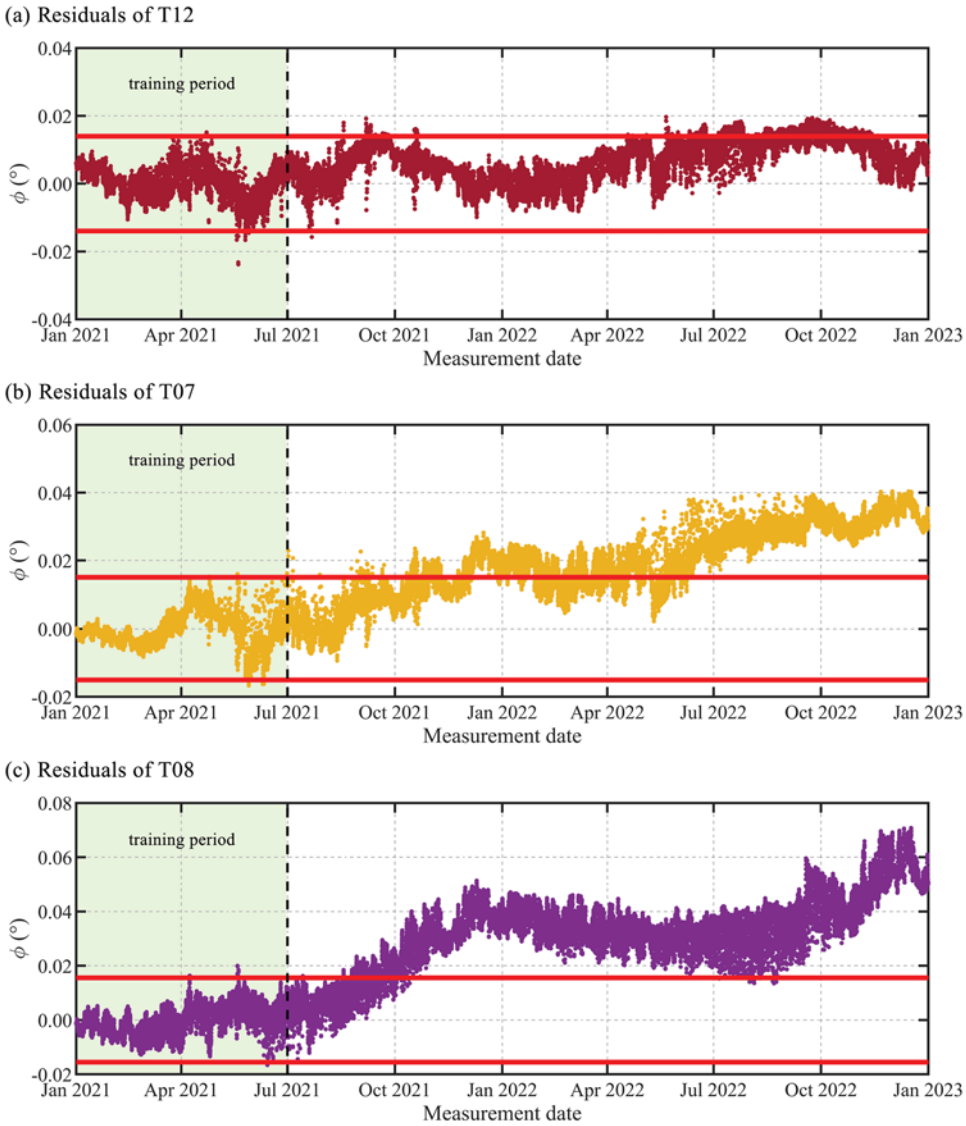

Fig. 20. Residuals of rotation T12, T07 and T08 with a $\pm 3\sigma_{\varphi}$ confidence interval.

- The expected normal behaviour is represented by tiltmeter T12 (Fig. 17a-b) and the corresponding features are: (a) no accumulation of rotation between January 2021 and December 2022 and (b) almost linear correlation between rotation and temperature (R^2 = 0.96).
- On the contrary, the tiltmeters on pier P06 – i.e. T07 (Fig. 17c-d) and T08 (Fig. 17e-f) – exhibit a series of anomalies: (a) the measured rotation reveals clear and increasing permanent rotation (about +0.05° for T07 and +0.07° for T08) and (b) the rotation-temperature correlation exhibits clear changes during the monitoring period.
- Behaviour in the middle of the previous two is experienced by T02 (Fig. 18a-b) and the tiltmeters on pier P04, i.e. T03 (Fig. 18c-d) and T04 (Fig. 18e-f): (a) the time evolution of measured rotations show an accumulation of rotation of about + 0.02° for T02, + 0.04° for T03 and + 0.05° for T04; (b) the rotations are linearly correlated with the outdoor temperature as shown by R^2 coefficient of 0.89 (T02), 0.86 (T03) and 0.91 (T04).

Table 2 illustrates the statistics of the measured rotations during the monitoring period in terms of average values (φ_{ave}), absolute maximum values ($\varphi_{|max|}$), standard deviations (σ_x) and coefficient of determination R^2 computed with respect to outdoor temperature θ1.

5.4. Novelty detection (on global rotations)

The anomaly detection is based on the residual errors between predicted and measured rotations. The predicted rotations are evaluated by using a simple linear regression model, with the temperature as its only input:

$$y_k = \alpha_0 + \alpha_1 \theta_k \quad (1)$$

where y_k is the output variable at instant k (i.e. the structural rotation at a certain location), θ_k is the measured temperature at instant k r temperature) and α_0, α_1 are the regression coefficients. The regression coefficients are determined using the rotation-temperature data collected during the training period represented by the first six months of monitoring. As it is usually done for natural frequencies [37], a different regression model was developed for each measured rotation.

Fig. 19 shows the histogram of measured rotations before and after removing the temperature effects through the adopted regression model: as it has to be expected, after applying the regression model, the rotations are concentrated in a narrower range. It is further noticed that approximately a normal distribution is obtained for rotation T12 (Fig. 19a), T02 (Fig. 19d) and T04 (Fig. 19f); on the contrary, the distribution of rotation T07 (Fig. 19b), T08 (Fig. 19c) and T03 (Fig. 19e)

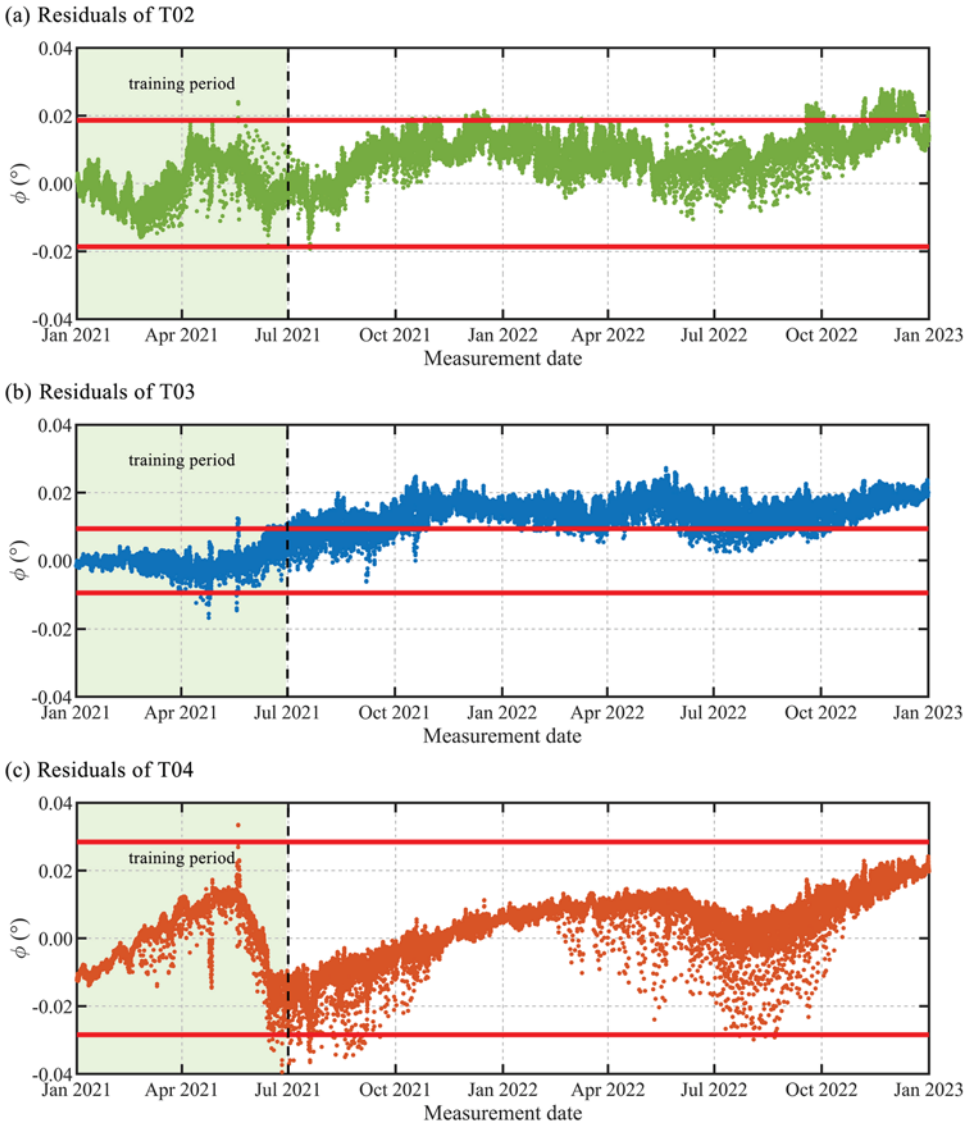

Fig. 21. Residuals of rotation T02, T03 and T04 with a $\pm 3\sigma_{\varphi}$ confidence interval.

exhibits two or more peaks.

Figs. 20 and 21 show the time evolution of residual errors. The control limits (i.e., the continuous red lines) were evaluated during the training period as $\pm 3\sigma_{\varphi}$. The residuals of T12 (Fig. 20a), T02 (Fig. 21a), and T04 (Fig. 21c) are generally included in the "safe" region, whereas the residual of T07 (Fig. 21b), T08 (Fig. 21c) and T03 (Fig. 21b) clearly exceeds the upper control limit. It is interesting to observe that the two tiltmeters T07 (Fig. 21b) and T08 (Fig. 21c) – mounted on pier P06 – exceed the control limits in different periods, suggesting that the permanent rotations are induced by arch deformations and not by pier settlements (i.e., not by scour).

According to Tubaldi et al. [7], the effects of scouring-induced settlements are related to pier-foundation rotations in the opposite direction of the river flow. In addition, the pier displacements start to increase beyond the values induced by vertical loads only after the maximum scour depth exceeds the foundation depth.

In the present case, tiltmeters T02, T03, T04, T07 and T08 experienced permanent rotation in the direction of the river flow; therefore, the phenomenon that caused the residual rotations should not be related to a soil settlement of the upstream side. It is worth mentioning that the distribution of vertical loads is not symmetric: the railway track – decommissioned in 2010 – is on the upstream side while the roadway is on the downstream side, causing an asymmetric distribution of service loads. In addition, it is recalled that tiltmeters installed on the same pier began to exhibit the permanent rotations at different times so that those rotations are most likely induced by the arch.

6. Conclusions

The paper focuses on the long-term monitoring performed in a historical masonry arch bridge, crossing the Sesia River in Northern Italy. Onsite inspections of the investigated bridge, called Candia bridge, revealed the presence of severe foundation erosion, mitigated by different interventions on the foundations and the riverbed. Furthermore, the documentary research has shown that the foundation level was deepened up to 12 m (measured from the plinth top), with the maximum measured depth of a scour hole being equal to 5.5 m.

The main aim of the monitoring system – including 15 tiltmeters and various sensors to measure the environmental effects, the water level and the riverbed elevation –is to detect scour-induced pier settlements. Variations in the structural behaviour of the bridge are measured by a series of MEMS tiltmeters installed at arch skewbacks, whereas the hydraulic actions were monitored through 1 hydrometer, 1 echosounder and 2 cameras.

Based on the results obtained in the first two years of monitoring (i.e., between 01/01/2020 and 31/12/2022), the following main conclusions can be drawn:

- Statistical analysis of the data collected during the first six months of monitoring revealed that 6 tiltmeters were measuring global rotations while 9 tiltmeters were measuring local rotations.
- The outdoor temperature turned out to be the dominant driver of the variations observed in the tilt measurements. Among the available temperature measurements, better rotation-temperature correlation is obtained using the thermistor integrated in tiltmeter T14.
- The relative humidity as well as the water elevation does not exhibit any correlation with the measured rotations. On the other hand, the maximum variation of water elevation, in the investigated monitoring period, ranged up to 3.6 m. Hence, the bridge seems not affected by relatively limited flood events.
- During the event of October 2021, an aggradation process was observed on the downstream side of pier P05.
- Various anomalies were detected in measured global rotations. The observed anomalies involves both the rise of increasing permanent rotations and the corresponding changes of the rotation-temperature correlation.
- As highlighted by the tiltmeters T07 and T8 installed on pier P06, the non-simultaneous increase of rotation toward the direction of river flow suggests to exclude that these anomalies are correlated with scour.
- The physical phenomenon that caused the observed permanent shifts in the rotation-temperature correlation is still unclear and onsite visual inspections are periodically performed to detect the onset of possible cracks in the arches.

The presented results highlight the difficulties in detecting scour-induced effects from the measure of pier rotations on masonry arch bridges. In more details, two issues can be identified: (1) distinguishing scour-induced rotations from other sources causing rotation changes; (2) measuring rotations with a very low amplitude. Regarding the first issue, a simple statistical analysis (discussed in Section 4) allows to distinguish the channels of data measuring the local rotations of the external arch ring and those measuring the rotations associated with the overall foundation-pier-arch system. Furthermore, tiltmeters should guarantee adequate accuracy and repeatability over time, and more redundancy in the measuring system might be desired. Consequently, a future upgrade in the monitoring system should involve the following improvements: (1) installing additional tiltmeters on the downstream side to help distinguish between the anomalies generated by the arches and by the piers-foundations; (2) installing additional tiltmeters at all the arch skewbacks; (3) the riverbed monitoring can be integrated with other buried probes (see, e.g. [12]) to increase the redundancy in the direct scour measure.

CRediT authorship contribution statement

Ballio Francesco: Writing – review & editing, Methodology, Conceptualization. **D'Angelo Manuel:** Writing – original draft, Methodology, Data curation. **Gentile Carmelo:** Writing – review & editing, Supervision, Methodology, Data curation, Conceptualization. **Borlenghi Paolo:** Writing – original draft, Software, Methodology, Investigation, Data curation.

Declaration of Competing Interest

The authors declare that they have no known competing financial interests or personal relationships that could have appeared to influence the work reported in this paper.

Data availability

Data will be made available on request.

Acknowledgments

The support of Regione Lombardia is gratefully acknowledged. Sincere thanks are due to G. Cazzulani, PhD (DMECC, Politecnico di Milano), G. Zonno, PhD (DABC, Politecnico di Milano), M. Cucchi and M. Iscandri (LPMSC, Politecnico di Milano) who assisted the authors during the installation of the monitoring system.

References

[1] K. Wardhana, F.C. Hadipriono, Analysis of recent bridge failures in the United States, J. Perform. Constr. Facil. 17 (3) (2003) 144–150, https://doi.org/10.1061/(ASCE)0887-3828(2003)17:3(144).
[2] NCHRP, Monitoring scour critical bridges – a synthesis of highway practice, Traffic Saf. Wash. DC (2009).
[3] R.J. Briaud, Real-time monitoring of bridge scour using remote monitoring technology, Tex. Transp. Inst. (2011).
[4] F. Ballio, A. Bianchi, S. Franzetti, F. De Falco, M. Mancini, Vulnerabilità idraulica dei ponti fluviali. In Atti XXVI Convegno Nazionale di Idraulica e Costruzioni Idrauliche, Catania, Italy Volume 3 (1998) 69–80.
[5] Z. van Leeuwen, R. Lamb, Flood and scour related failure incidents at railway assets between 1846 and 2013, Proj. W13-4224. JBA Trust 30 (2014) 20.
[6] P. Zampieri, M.A. Zanini, F. Faleschini, L. Hofer, C. Pellegrino, Failure analysis of masonry arch bridges subject to local pier scour, Eng. Fail. Anal. 79 (2017) 371–384, https://doi.org/10.1016/j.engfailanal.2017.05.028.
[7] E. Tubaldi, L. Macorini, B.A. Izzuddin, Three-dimensional mesoscale modelling of multi-span masonry arch bridges subjected to scour, Eng. Struct. 165 (2018) 486–500, https://doi.org/10.1016/j.engstruct.2018.03.031.
[8] S. Invernizzi, G. Lacidogna, A. Manuello, A. Carpinteri, AE monitoring and numerical simulation of a two-span model masonry arch bridge subjected to pier scour, Strain 47 (SUPPL. 2) (2011) 158–169, https://doi.org/10.1111/j.1475-1305.2010.00752.x.
[9] F. De Falco, R. Mele, The monitoring of bridges for scour by sonar and sedimetri, NDT E Int. 35 (2) (2002) 117–123, https://doi.org/10.1016/S0963-8695(01)00031-7.
[10] F. Ballio, G. Ballio, S. Franzetti, G. Crotti, G. Solari, Actions monitoring as an alternative to structural rehabilitation: case study of a river bridge, Struct. Control Health Monit. 25 (11) (2018), e2250, https://doi.org/10.1002/stc.2250.
[11] F. Larrarte, C. Chevalier, L. Battist, H. Chollet, Hydraulics and bridges: a French case study of monitoring of a bridge affected by scour, Flow. Meas. Instrum. 74 (2020), 101783, https://doi.org/10.1016/j.flowmeasinst.2020.101783.
[12] A. Maroni, E. Tubaldi, N. Ferguson, A. Tarantino, H. McDonald, D. Zonta, Electromagnetic sensors for underwater scour monitoring, Sensors 20 (15) (2020) 4096, https://doi.org/10.3390/s20154096.
[13] O. Link, M. García, A. Pizarro, H. Alcayaga, S. Palma, Local scour and sediment deposition at bridge piers during floods, J. Hydraul. Eng. 146 (3) (2020), 04020003, https://doi.org/10.1061/(ASCE)HY.1943-7900.0001696.
[14] Z. Li, F. Tang, Y. Chen, X. Hu, G. Chen, Y. Tang, Field experiment and numerical verification of the local scour depth of bridge pier with two smart rocks, Eng. Struct. 249 (2021), 113345, https://doi.org/10.1016/j.engstruct.2021.113345.
[15] L.A. Hempel, H.F. Malenda, J.W. Fulton, M.F. Henneberg, J.R. Cederberg, T. Moramarco, The applicability of time-integrated unit stream power for estimating bridge pier scour using noncontact methods in a Gravel-Bed River, Remote Sens. 14 (9) (2022) 1978, https://doi.org/10.3390/rs14091978.
[16] S. Foti, D. Sabia, Influence of foundation scour on the dynamic response of an existing bridge, J. Bridge Eng. 16 (2) (2011) 295–304, https://doi.org/10.1061/(ASCE)BE.1943-5592.0000146.
[17] F. Scozzese, L. Ragni, E. Tubaldi, F. Gara, Modal properties variation and collapse assessment of masonry arch bridges under scour action, Eng. Struct. 199 (2019), 109665, https://doi.org/10.1016/j.engstruct.2019.109665.
[18] W. Xiong, C.S. Cai, B. Kong, X. Zhang, P. Tang, Bridge scour identification and field application based on ambient vibration measurements of superstructures, J. Mar. Sci. Eng. 7 (5) (2019) 121, https://doi.org/10.3390/jmse7050121.
[19] A. Elsaid, R. Seracino, Rapid assessment of foundation scour using the dynamic features of bridge superstructure, Constr. Build. Mater. 50 (2014) 42–49, https://doi.org/10.1016/j.conbuildmat.2013.08.079.
[20] L.J. Prendergast, D. Hester, K. Gavin, Determining the presence of scour around bridge foundations using vehicle-induced vibrations, J. Bridge Eng. 21 (10) (2016), 04016065, https://doi.org/10.1061/(ASCE)BE.1943-5592.0000931.
[21] P.F. Lagasse, Bridge Scour and Stream Instability Countermeasures: Experience, selection, and design guidance. Hydraulic Engineering Circular No. 23, Third edition.,, Federal Highway Administration,, Washington, DC, 2009.
[22] W.F. Lee, T.T. Cheng, C.K. Huang, C.I. Yen, H.T. Mei, Performance of a highway bridge under extreme natural hazards: case study on bridge performance during the 2009 Typhoon Morakot, J. Perform. Constr. Facil. 28 (1) (2014) 49–60, https://doi.org/10.1061/(ASCE)CF.1943-5509.0000418.

[23] K. Faulkner, J.M.W. Brownjohn, Y. Wang, F. Huseynov, Tracking bridge tilt behaviour using sensor fusion techniques, J. Civ. Struct. Health Monit. 10 (4) (2020) 543–555, https://doi.org/10.1007/s13349-020-00400-9.
[24] F. Biondini, F. Ballio, M. di Prisco, S. Bianchi, M. D'Angelo, G. Zani, L. Capacci, M. Anghileri, A. Scalbi, K. Flores Ferreira, Bridge vulnerability and hazard assessment for risk-based infrastructure management, in: J.R. Casas, et al. (Eds.), Bridge Safety, Maintenance, Management, Life-Cycle, Resilience and Sustainability, CRC Press, 2002, https://doi.org/10.1201/9781003322641-231.
[25] M.P. Limongelli, C. Gentile, F. Biondini, M. di Prisco, F. Ballio, G. Zonno, P. Borlenghi, S. Bianchi, L. Capacci, M. Anghileri, G. Zani, A. Scalbi, K.F. Ferreira, M. D'Angelo, G. Cazzulani, L. Benedetti, C. Somaschini, L. Bernardini, M. Belloli, F. Resta, P. Vigo, A. Colombo, Bridge structural monitoring: the Lombardia regional guidelines, Struct. Infrastruct. Eng. (2022), https://doi.org/10.1080/15732479.2022.2107023.
[26] P. Borlenghi, M. D'Angelo, F. Ballio, C. Gentile, Continuous Monitoring of Masonry Arch Bridges to Evaluate the Scour Action, in: C. Pellegrino, et al. (Eds.), *Proceedings of the 1st Conference of the European Association on Quality Control of Bridges and Structures*, EUROSTRUCT 2021. Lecture Notes in Civil Engineering, vol 200, Springer, Cham, 2022, https://doi.org/10.1007/978-3-030-91877-4_46.
[27] P. Borlenghi, C. Gentile, G. Zonno, Monitoring Reinforced Concrete Arch Bridges with Operational Modal Analysis, in: C. Pellegrino, et al. (Eds.), *Proceedings of the 1st Conference of the European Association on Quality Control of Bridges and Structures*, EUROSTRUCT 2021. Lecture Notes in Civil Engineering, vol 200, Springer, Cham, 2022, https://doi.org/10.1007/978-3-030-91877-4_42.
[28] S. Bianchi, F. Biondini, M. D'Angelo, F. Ballio, M. Anghileri, G. Rosati, G. Cazzulani, Satellite-Based Structural and Hydraulic Monitoring of a 50-Year-Old Bridge over the Oglio River in Italy, in: C. Pellegrino, et al. (Eds.), Proceedings of the 1st Conference of the European Association on Quality Control of Bridges and Structures, EUROSTRUCT 2021. Lecture Notes in Civil Engineering, vol 200, Springer, Cham, 2022, https://doi.org/10.1007/978-3-030-91877-4_44.
[29] S. Bianchi, F. Biondini, G. Rosati, M. Anghileri, L. Capacci, G. Cazzulani, L. Benedetti, Structural Health Monitoring of Two Road Bridges in Como, Italy, in: C. Pellegrino, et al. (Eds.), *Proceedings of the 1st Conference of the European Association on Quality Control of Bridges and Structures*, EUROSTRUCT 2021. Lecture Notes in Civil Engineering, vol 200, Springer, Cham, 2022, https://doi.org/10.1007/978-3-030-91877-4_45.
[30] M. D'angelo, A. Menghini, P. Borlenghi, L. Bernardini, L. Benedetti, F. Ballio, M. Belloli, C. Gentile, Hydraulic safety evaluation and dynamic investigations of Baghetto Bridge in Italy, Infrastructures 7 (4) (2022) 53, https://doi.org/10.3390/infrastructures7040053.
[31] A. Pizarro, S. Manfreda, E. Tubaldi, The science behind scour at bridge foundations: a review, Water 12 (2) (2020) 374, https://doi.org/10.3390/w12020374.
[32] L. Martinengo, Ponte in muratura sul fiume Sesia nella ferrovia in costruzione di Asti-Casale-Mortara, Regia Sc. d'Applicazione per gli Ing. di Torino (1869).
[33] International Union of Railways, UIC (2020) Catalogue of Damages in masonry arch bridges. Paris, France.
[34] G. Curioni, L'arte del costruire: costruzioni civili, stradali ed idrauliche (in Italian), Augusto Feder Negro Ed. Turin (1873).
[35] G. Crotti, A. Cigada, Scour at river bridge piers: real-time vulnerability assessment through the continuous monitoring of a bridge over the river Po, Italy, J. Civ. Struct. Health Monit. 9 (4) (2019) 513–528, https://doi.org/10.1007/s13349-019-00348-5.
[36] D.S. Moore, W.I. Notz, M.A. Flinger, The Basic Practice of Statistics, W. H. Freeman and Company, 2013.
[37] F. Magalhães, A. Cunha, E. Caetano, Vibration based structural health monitoring of an arch bridge: from automated OMA to damage detection, Mech. Syst. Signal Process. 28 (2012) 212–228, https://doi.org/10.1016/j.ymssp.2011.06.011.